

Available online at www.sciencedirect.com



Trans. Nonferrous Met. Soc. China 21(2011) 2559-2567

Transactions of **Nonferrous Metals Society of China**

www.tnmsc.cn

Corrosion mechanism associated with Mg₂Si and Si particles in Al-Mg-Si alloys

ZENG Feng-li¹, WEI Zhong-ling², LI Jin-feng¹, LI Chao-xing¹, TAN Xing¹, ZHANG Zhao³, ZHENG Zi-qiao¹

- 1. School of Materials Science and Engineering, Central South University, Changsha 410083, China;
 - 2. Jiaxing Key Laboratory of Light Alloy Technology, Jiaxing 314051, China;
 - 3. Department of Chemistry, Zhejiang University, Hangzhou 310027, China

Received 24 December 2010; accepted 15 April 2011

Abstract: The electrochemical behaviors and coupling behaviors of the Mg₂Si and Si phases with α (Al) were investigated, the corrosion morphologies of Al alloys containing Mg₂Si and Si particles were observed, and the corrosion mechanism associated with them in Al-Mg-Si alloys was advanced. The results show that Si particle is always cathodic to the alloy base, Mg₂Si is anodic to the alloy base and corrosion occurs on its surface at the beginning. However, during its corrosion process, the preferential dissolution of Mg and the enrichment of Si make Mg₂Si transform to cathode from anode, leading to the anodic dissolution and corrosion of the alloy base at its adjacent periphery at a later stage. As the mole ratio of Mg to Si in an Al-Mg-Si alloy is less than 1.73, it contains Mg₂Si and Si particles simultaneously in the grain boundary area, and corrosion initiates on the Mg₂Si surface and the precipitate-free zone (PFZ) at the adjacent periphery of Si particle. As corrosion time is extended, Si particle leads to severe anodic dissolution and corrosion of the PFZ at its adjacent periphery, expedites the polarity transformation between Mg₂Si and the PFZ and accelerates the corrosion of PFZ at the adjacent periphery of Mg₂Si particle.

Key words: Al-Mg-Si alloys; intergranular corrosion; corrosion mechanism; electrochemical behaviors; Mg₂Si; Si

1 Introduction

6xxx series [AlMgSi(Cu)] Al alloys are generally considered to be corrosion resistant although they can be susceptible to intergranular corrosion, and it was proposed that this could be caused by Si concentration in excess of the Mg₂Si ratio, precipitation of elemental Si or Cu-containing phases [1], or the anodic dissolution of the intermetallic phase Mg₂Si, along grain boundaries [2].

Precipitates or particles play an important role in the local distribution and rate of cathodic and anodic reactions. For Al-Mg-Si alloys, aging precipitates and grain boundaries are seen as the main anodic corrosion initiation sites, and most precipitates enhance the corrosion rate due to their cathodic activity [3-5]. It was claimed that intergranular corrosion susceptibility was the result of microgalvanic coupling between AlCu, CuSi or (Al) MgSiCu grain boundary precipitates and the adjacent precipitate-free zone (PFZ). β-phase (Mg₂Si) and pure Si particle may precipitate if the Mg/Si mole ratio is lower than 1.73. Some researchers suggested that grain boundary precipitates of the β -phase are not associated with intergranular corrosion (IGC) susceptibility, unless present as a continuous film [6-8]. There have been many researches concerning preparation and processing of the Al alloys containing Mg₂Si particles. However, the exact nature and properties of these precipitates in relation to IGC were not reported [9]. WANG and TIAN [10] presented that Al-Mg-Si alloys with a mole ratio of Mg to Si higher than 1.73 are not sensitive to intergranular corrosion due to little potential difference between Mg₂Si particle and Al matrix. However, BIRBILIS et al [11] found that the corrosion potential of Mg₂Si particles was much negative with respect to that of aluminum alloy matrix in 0.1 mol/L NaCl solution. The potential of 6xxx series Al alloy matrix is from about -0.72 V to -0.75 V (vs SCE) and that of Mg₂Si particles is about -1.54 V in NaCl solution [12]. According to BIRBILIS's result, it can be

deduced that the Al-Mg-Si alloy with a mole ratio of Mg to Si higher than 1.73 should be sensitive to IGC. This is obviously contradictory to our understanding of the corrosion behavior of 6xxx series Al alloy.

The purpose of the present study is to clarify the corrosion mechanism associated with the grain boundary precipitates of Mg_2Si and Si in Al-Mg-Si alloy. Their electrochemical behavior and coupling behavior with $\alpha(Al)$ (corresponding to grain boundary PFZ) were investigated, and the corrosion morphologies of the Al alloys containing coarse Mg_2Si and particles were observed. The corresponding corrosion mechanism was advanced.

2 Experimental

2.1 Preparation of simulated Mg₂Si phase

The Mg₂Si powder was manufactured through solid state reaction at 450 °C for 40 h according to its chemical proportion. The synthesized powder was identified through X-ray diffraction (XRD). Then, the Mg₂Si powder was sintered through plasma sintering at 900 °C for 10 min under compressive pressure of 30 MPa. In addition, the aluminum alloy matrix or grain boundary precipitation free zone contains low content of alloying elements, which can be replaced by $\alpha(Al)$ to undergo electrochemical tests.

2.2 Electrochemical measurement and coupling behavior of associated phases

The specimens for electrochemical measurement were cut from $\alpha(Al)$, the bulk Mg₂Si and Si. They were connected to a copper wire, and mounted in epoxy resin with an exposed surface, respectively. The exposed surface was ground using abrasive papers through 500-grade to 1200-grade, polished with Cr₂O₃ powder, rinsed using acetone, degreased with distilled water and then dried in air. After 10 min of immersion in a 3.5% NaCl solution, their potentiodynamic scanning curves were measured with a CHI660 electrochemical workstation at a scanning rate of 1 mV/s. During the measurement, the working electrode was the specimens, a large platinum sheet and a saturated calomel electrode (SCE) with a Luggin capillary served as counter and reference electrodes, respectively.

Meanwhile, the bulk Mg_2Si and Si were coupled separately or simultaneously with $\alpha(Al)$ in the 3.5% NaCl solution, and the coupling method was shown in our previous paper [13–14], as shown in Fig. 1. During the coupling test, the coupling current was measured. In the coupled system, the area of the Mg_2Si , $\alpha(Al)$ and Si were 28.26, 24 and 10.17 mm², respectively. After 312 h, the coupling test was finished, the coupled electrodes were disconnected, and the open circuit potential of

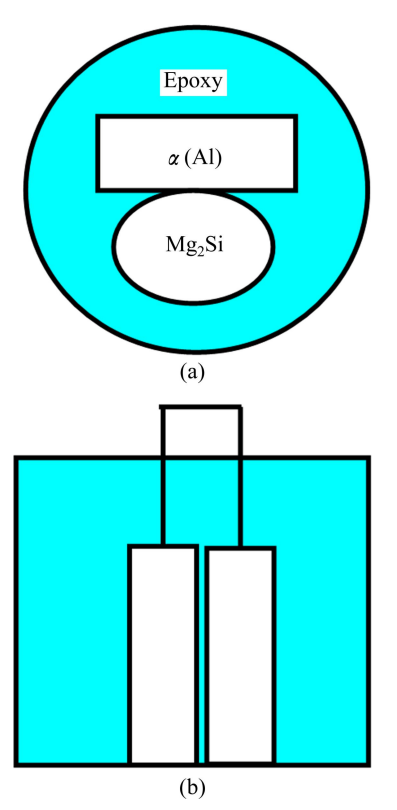


Fig. 1 Schematic diagram of coupling system: (a) Top view; (b) Lateral view

corresponding electrode was measured with the CHI660 electrochemical workstation.

2.3 Potential distribution in Al-Mg-Si alloy with different ratios of Mg to Si

Two Al-Mg-Si alloys with chemical composition of Al-0.63Mg-0.28Si and Al-0.63Mg-0.88Si were prepared, of which the mole ratios of Mg to Si are higher than 1.73 and lower than 1.73, respectively. After solution treatment, the alloy sheet was quenched followed by aging at 175 °C for 1 h. The alloy surface was ground using abrasive papers through 500-grade to 1200-grade, polished with Cr₂O₃ powder, rinsed using acetone, degreased with distilled water and then dried in air. Then, the potential distribution associated with the phases in the area of the grain boundary was mapped through a Nano Scope IIIa atomic force microscope (AFM).

2.4 Preparation of Al alloys containing corresponding coarse particles and their corrosion morphologies

The corrosion morphologies associated with the aging precipitates in real Al alloys could not been recognized by SEM due to their too small size. To clearly observe the corrosion morphologies associated with the Mg₂Si and Si particles by SEM, two Al alloys containing these particles were made through melting and casting.

One alloy contained Mg_2Si particle, and the other contained Mg_2Si and Si particles simultaneously. In these Al alloys, the Mg content was higher than 5% (mass fraction). After casting, the cast ingot was annealed at 450 °C for 24 h and cooled in the oven. Therefore, the Mg_2Si and Si particles in these alloys were greatly coarsened, then the corrosion morphologies could be distinguished with SEM.

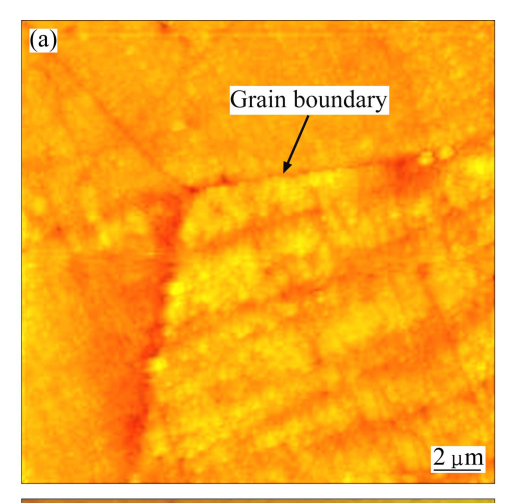
The surfaces of these Al alloys were ground using abrasive papers through 400-grade to 1000-grade, polished with diamond paste, rinsed using acetone, degreased with distilled water and dried in air. Then, they were immersed in the prepared NaCl solution for 12 h. To clearly distinguish the corrosion morphology of the simulated Al alloy, the corrosion product covering on the surface was removed using 2% CrO₃+5% H₃PO₄ solution at 80 °C, and the corresponding corrosion morphologies were observed with the Sirion200 SEM.

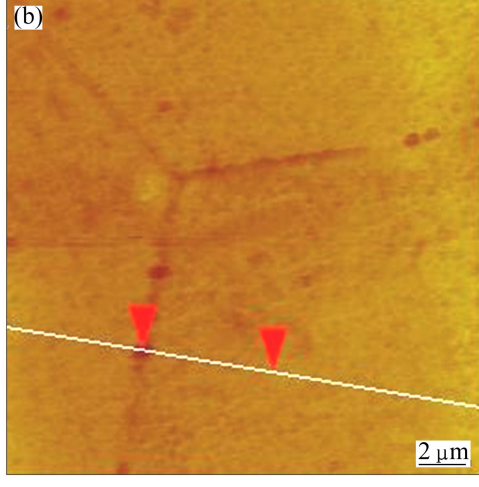
3 Results and discussion

The AFM images of grain boundary in the Al-0.63Mg-0.28Si (n(Mg)/n(Si)>1.73) alloy are shown in Fig. 2. The Mg₂Si particles distributed on the boundary are distant from each other (Fig. 2(a)). The dark regions in the potential distribution map (Fig. 2(b)) are related to Mg₂Si particles with more negative potential and there exists a potential difference as high as 180 mV (Fig. 2) between the grain boundary Mg₂Si particles and Al base. AFM images of grain boundary in the Al-0.63Mg-0.88Si (n(Mg)/n(Si)<1.73)alloy are shown in Fig. 3. Si particles (whiter dots) and Mg₂Si particles (darker dots) at the grain boundary can be distinguished (Fig. 3(a)). As can be seen in the potential distribution curve (Fig. 3(b)), Si has the most positive potential, followed by Al base, while Mg₂Si comes the last (Fig. 3(c)). The potential difference between Si and Al base is 180 mV. While, the potential difference between Si and the Mg₂Si is up to 269 mV. The potential measurement result through AFM is consistent with that measured through electrochemical method.

Figure 4 shows the XRD pattern of the synthesized Mg_2Si powder. It shows that the powder almost consists of single-phased Mg_2Si . The sintered bulk Mg_2Si could substitute for the real aging precipitate of Mg_2Si in Al-Mg-Si alloy to undergo electrochemical measurement. Meanwhile, $\alpha(Al)$ could substitute for the precipitate-free zone or the alloy base, due to its extremely little alloying element.

The potentiodynamic scanning curves and the corresponding corrosion parameters of individual $\alpha(Al)$, Mg₂Si and Si are presented in Fig. 5 and Table 1, respectively. It is clearly seen that the corrosion potential (φ_{corr}) of Mg₂Si is the most negative, while that of Si is





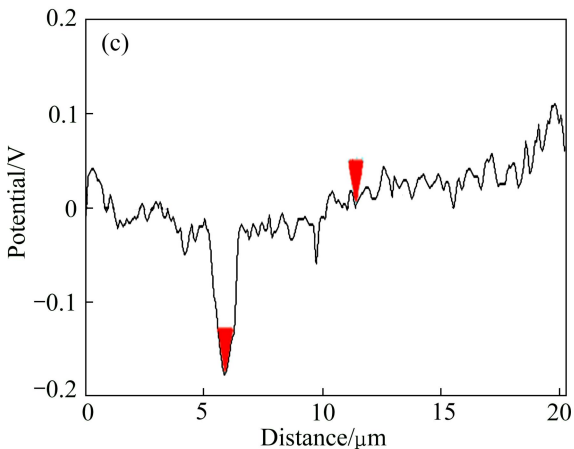


Fig. 2 AFM observation of grain boundary in Al-0.63Mg-0.28Si alloy: (a) AFM morphology; (b) Potential distribution; (c) Potential distribution curve along straight line in Fig. 2(b)

the most positive. This is consistent with the AFM measurement result. The polarization resistance (R_P) of $\alpha(Al)$ or Mg₂Si is less than that of Si. Meanwhile, the corrosion current density (J) of Mg₂Si is much greater than that of $\alpha(Al)$ or Si. These results indicate that Mg₂Si particles are more susceptible to corrosion than $\alpha(Al)$ or Si particles at the beginning.

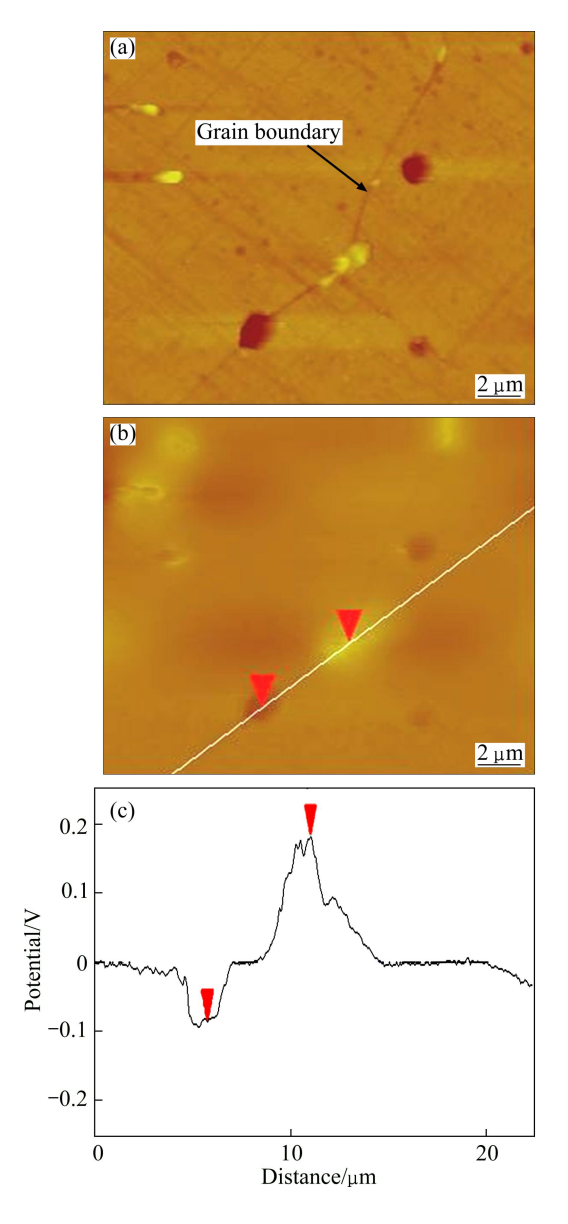


Fig. 3 AFM observation of grain boundary in Al-0.63Mg-0.88Si alloy: (a) AFM morphology; (b) Potential distribution; (c) Potential distribution curve along straight line in Fig. 3(b)

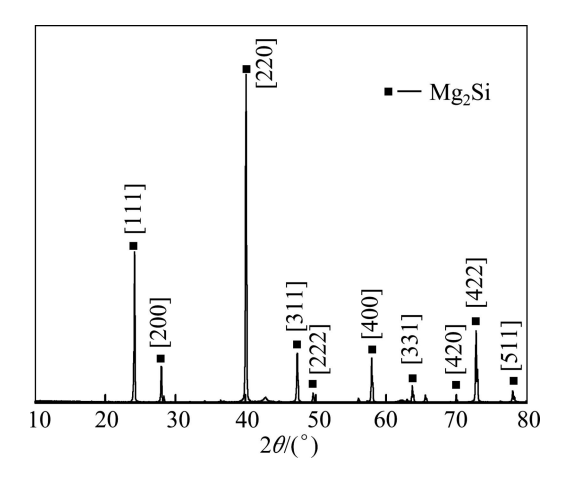


Fig. 4 XRD pattern of synthesized Mg₂Si powder

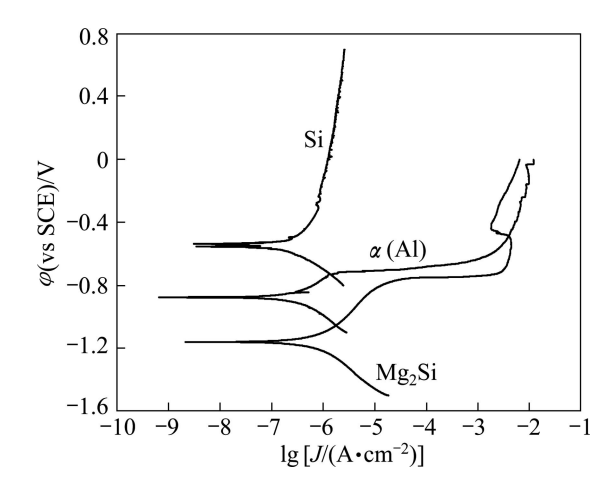


Fig. 5 Potentiodynamic scanning curves of individual α (Al), Si and Mg₂Si in 3.5% NaCl solution at the beginning

Table 1 Corrosion parameters of α (Al), Si and Mg₂Si in 3.5% NaCl solution at the beginning

Phase	$\varphi_{\rm corr}({ m vs~SCE})/{ m V}$	$J/(\text{A}\cdot\text{cm}^{-2})$	$R_{\rm P}/(\Omega\cdot{\rm cm}^2)$
α(Al)	-0.8761	7.674×10^{-7}	3.399 4×10 ⁴
Mg_2Si	-1.1598	1.282×10^{-6}	$2.034\ 2\times10^4$
Si	-0.5470	1.912×10^{-7}	$1.364~4\times10^{5}$

For the $Mg_2Si-\alpha(Al)$ coupling system, after coupling for 312 h in NaCl solution, the potentiodynamic scanning curves of $\alpha(A1)$ and Mg₂Si are shown in Fig. 6. It is found that the open circuit potential of Mg₂Si moves towards a positive direction to about -0.62 V(vs SCE) from the initial about -1.16 V, resulting in the potential order variation of Mg₂Si and α (Al), and a polarity transformation is generated. The potential of Mg₂Si electrode moves to a positive direction, which is due to the preferential dissolution of active Mg elements and the enrichment of Si. Energy spectrum of Mg₂Si phase after coupling for 312 h showed that Mg content was decreased, while Si content was increased. The preferential dissolution phenomenon was also found in S(Al₂CuMg) particle in 2024 Al alloy. BUCHHEIT et al [15], SHAO et al [16], and LI et al [17] found that as 2xxx series Al alloy containing S(Al₂CuMg) particle was immersed in NaCl solution, active Mg element in the S particle was preferentially dissolved, resulting in Cu-rich remnants.

The open circuit potential order change of the $Mg_2Si-\alpha(Al)$ coupled system will cause the coupling current variation, as shown in Fig. 7. At the beginning of the coupling process, the potential of Mg_2Si electrode is negative to that of $\alpha(Al)$ electrode, indicating that Mg_2Si electrode acts as anode and endures anodic current. During the coupling process, its potential moves to a positive direction with increasing immersion time. As a

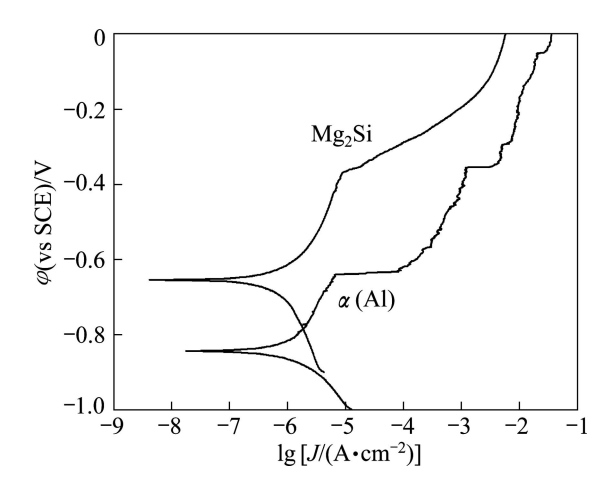


Fig. 6 Potentiodynamic scanning curves of $\alpha(Al)$ and Mg₂Si in Mg₂Si- $\alpha(Al)$ coupling system after coupling for 312 h in NaCl solution

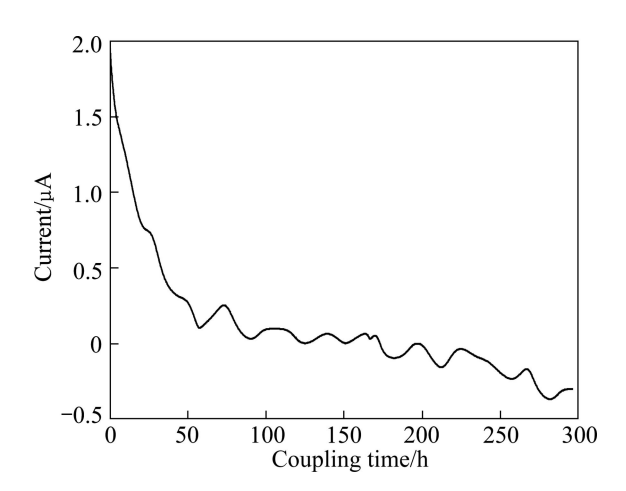


Fig. 7 Coupling current of Mg₂Si with $\alpha(Al)$ in 3.5% NaCl solution

result, the corroded Mg_2Si becomes cathodic to the $\alpha(Al)$ electrode at a later stage, and the anodic current of Mg_2Si electrode changes to cathodic current and increases.

For the $Mg_2Si-\alpha(Al)-Si$ coupling system, the potentiodynamic scanning curves of individual $\alpha(Al)$, Si and Mg_2Si after coupling for 312 h in the NaCl solution are shown in Fig. 8. The open circuit potential order change of Mg_2Si , $\alpha(Al)$ and Si in the three-electrode coupling system is also observed. The electrode potential of $\alpha(Al)$ and Mg_2Si is still negative with respect to that of Si. However, the potential of Mg_2Si electrode moves to a positive direction, resulting in the potential of $\alpha(Al)$ being negative to that of Mg_2Si phase and Si phase. Energy spectrum also showed the preferential dissolution of Mg_2Si electrode.

The open circuit potential order change of the $Mg_2Si-\alpha(Al)-Si$ coupling system also causes the coupling current variation, as shown in Fig. 9(a). During all the coupling process, Si electrode always acts as

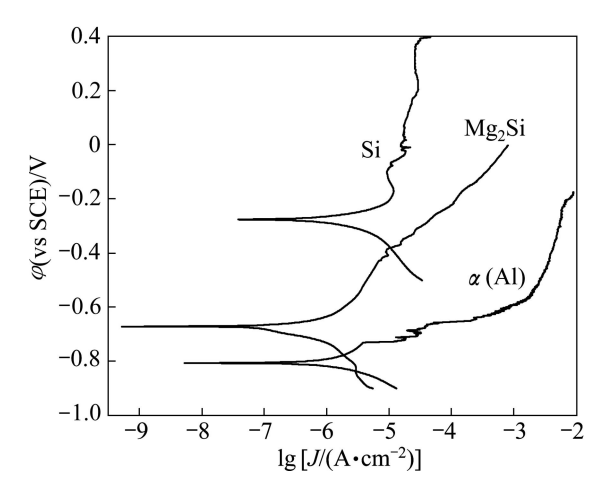


Fig. 8 Potentiodynamic scanning curves of individual $\alpha(Al)$, Si and Mg₂Si in Mg₂Si- $\alpha(Al)$ -Si coupling system after coupling for 312 h in NaCl solution

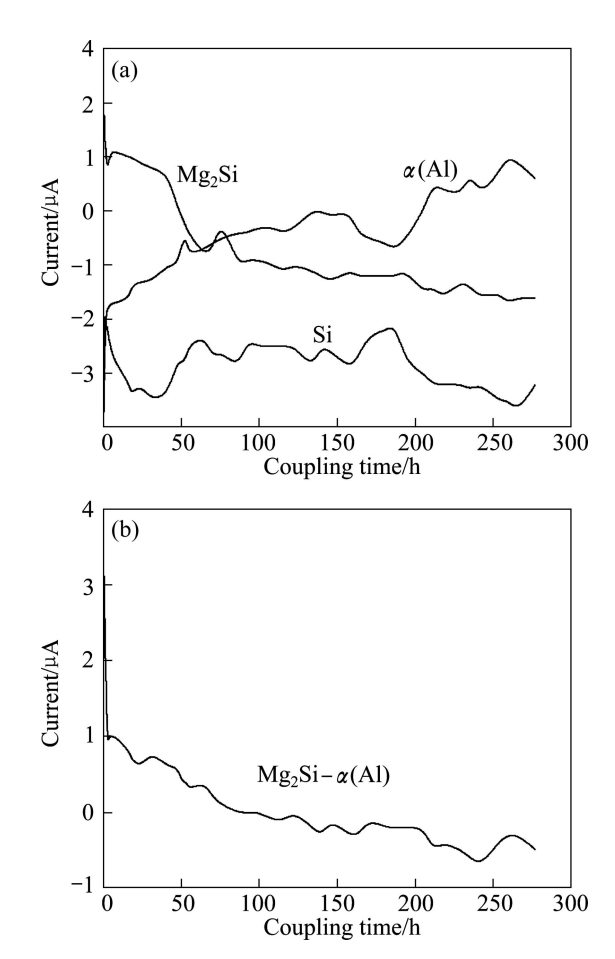


Fig. 9 Coupling current of Mg₂Si, Si and α (Al) in Mg₂Si– α (Al)–Si coupling system: (a) Coupling current of Mg₂Si, Si and α (Al); (b) Coupling current of Mg₂Si– α (Al)

cathode and endures cathodic current. At the beginning, Mg_2Si electrode acts as the only anode and endures anodic current. With increasing the coupling time, its potential moves to a positive direction, as a result, the corroded Mg_2Si electrode becomes cathodic to $\alpha(Al)$

electrode at a later stage, leading to the anodic current of Mg₂Si electrode changing to cathodic current and increasing. While the $\alpha(Al)$ electrode acts as cathode and endures cathodic current at the beginning, its cathodic current is changed to anodic current and increases with increasing the coupling time. At a later stage, the $\alpha(Al)$ electrode acts as the only anode and endures all anodic current. Due to the potential order change, during the coupling intervals of the Mg₂Si- $\alpha(Al)$ -Si coupling system, as only Mg₂Si and $\alpha(Al)$ are coupled, the anodic current of Mg₂Si electrode changes to cathodic current and increases, as shown in Fig. 9(b).

For both the $Mg_2Si-\alpha(Al)$ two-electrode coupling system and the $Mg_2Si-\alpha(Al)-Si$ three-electrode coupling system, there exists an electrochemical polarity transformation process between Mg_2Si electrode and $\alpha(Al)$ electrode. However, the beginning time of electrochemical polarity transformation is different. In the $Mg_2Si-\alpha(Al)$ coupling system, after coupling for about 100 h, the cathodic current of $\alpha(Al)$ electrode changes to anodic current (Fig. 7). While, in the $Mg_2Si-\alpha(Al)-Si$ coupling system, the beginning time when the cathodic current of $\alpha(Al)$ electrode changes to anodic current is decreased to about 50 h (Fig. 9). In addition, compared with that in $Mg_2Si-\alpha(Al)$ coupling system, $\alpha(Al)$ electrode endures higher anodic current in the $Mg_2Si-\alpha(Al)-Si$ at the later stage.

Figure 10 shows the corrosion morphologies of Al alloys containing coarse Mg₂Si particles and Mg₂Si+Si particles immersed in 3.5% NaCl solution for 0.5 h. It is seen that the corrosion occurs on Mg₂Si particle surface of these two alloys. No corrosion occurs on Si particle surface, but corrosion occurs on the Al base at the adjacent periphery of Si particle.

The corrosion morphologies of these two Al alloys immersed in 3.5% NaCl solution for 2 h are shown in Fig. 11. In the Al alloy only containing coarse Mg₂Si particle, corrosion occurs on the Mg₂Si particle surface. It is also observed that corrosion occurs on the Al base at its adjacent periphery (Fig. 11(a)). The EDS spectrum (Fig. 11(b)) shows that the Mg content is decreased, while the Si content in the corroded Mg₂Si particle is increased to 52.13%, which is higher than the original Si content of the Mg₂Si particle. In the Al alloy containing coarse Mg₂Si and Si particles, severe corrosion occurs on the Al base at the adjacent periphery of Si particle (Fig. 11(c)). Meanwhile, corrosion is observed on the Mg₂Si particle surface and also on the Al base at its adjacent periphery. Correspondingly, EDS spectrum (Fig. 11(d)) shows that the Si content in the Mg₂Si particle is greatly increased to about 79%.

As the immersion time is extended, the corrosion on Al base at the adjacent periphery of the Mg₂Si particle is due to the preferential dissolution of Mg in the Mg₂Si

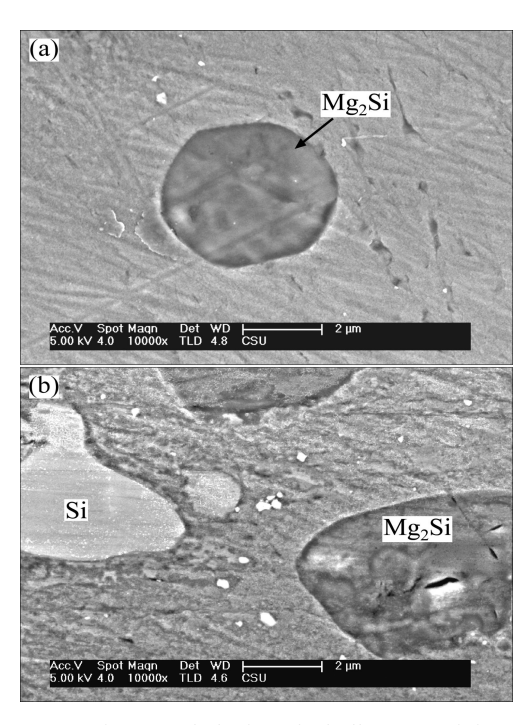


Fig. 10 Corrosion morphologies of Al alloys containing coarse particles immersed in 3.5% NaCl solution for 0.5 h: (a) Mg_2Si particle; (b) Mg_2Si+Si particles

particle and the electrochemical polarity transfer, which is consistent with the above coupling test. That is to say, there exists a dynamic conversion corrosion mechanism associated with the Mg₂Si particle. At the beginning, the Mg₂Si particle is anodic to the Al base and corrosion occurs on its surface. However, during its corrosion process, its potential moves to a positive direction with increasing immersion time, due to the preferential dissolution of Mg and the enrichment of Si. As a result, the corroded Mg₂Si particle becomes cathodic to the Al base at a later stage, leading to the anodic dissolution and corrosion of the Al base at its adjacent periphery.

The above corrosion morphologies also indicate that the corrosion occurs firstly on the Mg₂Si particle surface and develops on the Al base at its adjacent periphery in the Al alloy containing only Mg₂Si particle. However, in the Al alloy containing Mg₂Si and Si particles, the corrosion begins on the Mg₂Si particles surface and the Al base at the adjacent periphery of Si particle. Then, the corrosion develops on the Al base at the adjacent periphery of Si particle, and also develops on the Al base at the adjacent periphery of Mg₂Si particle. Compared with that at Mg₂Si adjacent periphery, the corrosion degree of Al base at Si adjacent periphery is much higher. In addition, the Si enrichment of the corroded Mg₂Si particles in the Al alloy containing coarse Mg₂Si and Si particles is more server than that in the Al alloy containing only Mg₂Si particle. It indicates that existence of Si particles enhances the preferential dissolution of

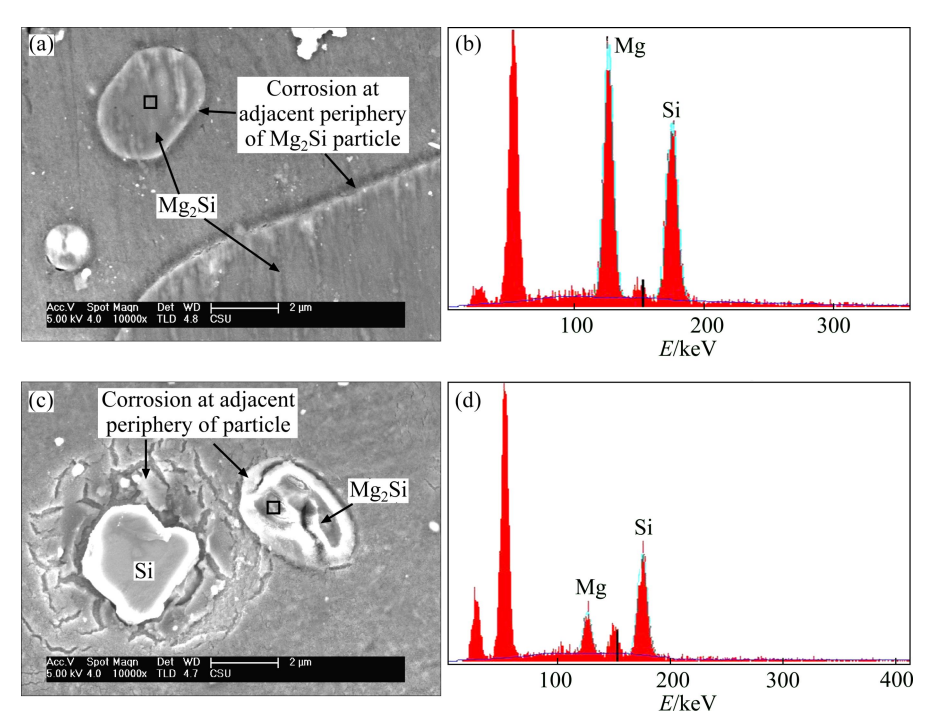


Fig. 11 Corrosion morphologies and corresponding EDS spectra of Al alloys containing coarse particles immersed in 3.5% NaCl solution for 2 h: (a), (b) Mg₂Si particle; (c), (d) Mg₂Si+Si particles

Mg and the enrichment of Si during the corrosion process of Mg₂Si particle.

According to the above results and discussion, the intergranular corrosion mechanism of Al-Mg-Si alloys with different mole ratios of Mg to Si was advanced, as shown in Figs. 12 and 13. In the Al-Mg-Si alloys with a mole ratio of Mg to Si higher than 1.73, only Mg₂Si is precipitated at the grain boundary. There exists a dynamic conversion corrosion mechanism associated with the precipitate of Mg₂Si. At the beginning, the precipitate of Mg₂Si is anodic to the alloy base (or precipitate-free zone, PFZ) and corrosion occurs on its surface (Fig. 12(b)). However, during its corrosion process, its potential moves to a positive direction with increasing corrosion time, due to the preferential dissolution of Mg and the enrichment of Si in Mg₂Si precipitate. As a result, the corroded Mg₂Si phase becomes cathodic to the PFZ at the grain boundary at a later stage, leading to the anodic dissolution and corrosion of the PFZ at its adjacent periphery (Fig. 12(c)). That is to say, the corrosion develops along the PFZ at the adjacent periphery of Mg₂Si precipitate. Because the Mg₂Si precipitates at the grain boundary are distributed discontinuously, there is no continuous corrosion channel at the grain boundary. Therefore, the Al-Mg-Si alloy with the mole ratio of Mg to Si higher than 1.73 is not susceptible to intergranular corrosion.

In the Al-Mg-Si alloys with a mole ratio of Mg to Si less than 1.73, Mg₂Si and Si precipitate at the grain boundary simultaneously. At the initial corrosion stage,

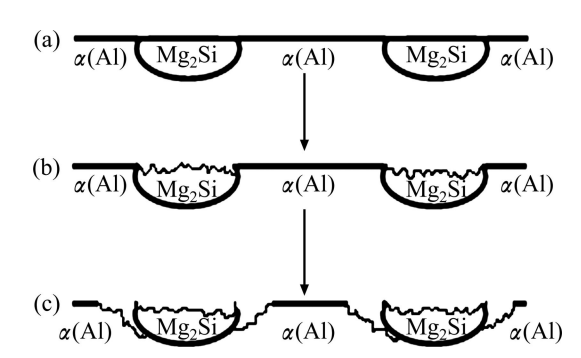


Fig. 12 Schematic diagram of function mechanism of Mg_2Si precipitate in intergranular corrosion of Al-Mg-Si alloys with n(Mg)/n(Si) > 1.73: (a) Mg_2Si particles along grain boundary; (b) Corrosion initiation on Mg_2Si surface at the beginning; (c) Corrosion of PFZ at adjacent periphery of corroded Mg_2Si particles at a later stage

the corrosion potential of Mg_2Si is negative with respect to that of $\alpha(Al)$ or Si, so the corrosion mainly occurs on the Mg_2Si particles surface firstly. Meanwhile, the cathodic Si particle also leads to the anodic dissolution and corrosion of the PFZ at its adjacent periphery. That is to say, the corrosion initiates at grain boundary Mg_2Si particle and also at the grain boundary PFZ at Si particle adjacent periphery, as shown in Si is a cathodic zone. The anodic dissolution and corrosion of the grain boundary PFZ at its adjacent periphery are increased with increasing immersion time (Fig. 13(c)). Meanwhile, the cathodic Si particles accelerate the preferential

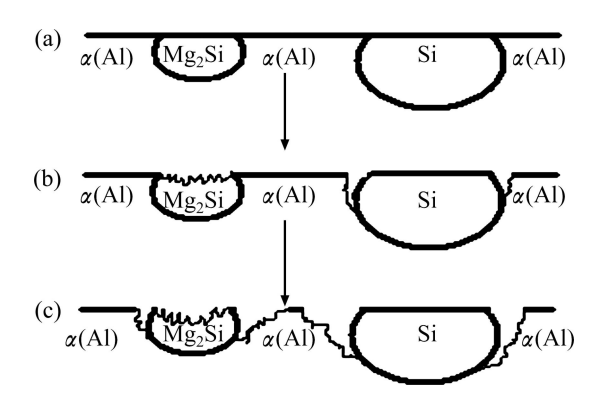


Fig. 13 Schematic diagram of function mechanism of Mg₂Si and Si precipitates in intergranular corrosion of Al–Mg–Si alloys with n(Mg)/n(Si) < 1.73; (a) Mg₂Si and Si particles along grain boundary; (b) Corrosion initiation on Mg₂Si surface and on PFZ at adjacent periphery of Si particle at the beginning; (c) Corrosion of PFZ at adjacent periphery of corroded Mg₂Si and Si particles at a later stage

dissolution of Mg and the enrichment of Si in Mg₂Si precipitates, and expedite the polarity transformation between Mg₂Si and the grain boundary PFZ. Therefore, the electrochemical driving force for anodic dissolution of the PFZ at the adjacent periphery of Mg₂Si precipitate is increased, and the corrosion of the PFZ at the adjacent periphery of Mg₂Si precipitate is enhanced. That is to say, the corrosion develops along the grain boundary PFZ at the adjacent periphery of both the Si particles and the corroded Mg₂Si precipitates, as shown in Fig. 13(c). The Si particles lead to the sever-corrosion development of the PFZ at its adjacent periphery, which accelerates the corrosion of the PFZ at the adjacent periphery of Mg₂Si precipitates. Even though the Mg₂Si precipitates are distributed discontinuously at the grain boundary, there also can form a continuous corrosion channel.

4 Conclusions

- 1) At the beginning of corrosion process, the precipitate of Mg_2Si is anodic to the Al base, and the anodic dissolution and corrosion occur on its surface. However, during its corrosion process, active Mg is preferentially dissolved, resulting in the enrichment of Si, which makes Mg_2Si potential move to a positive direction. As a result, the corroded Mg_2Si becomes cathodic to $\alpha(Al)$, leading to the anodic dissolution and corrosion of the Al base at its adjacent periphery at a later stage.
- 2) At the grain boundary of Al-Mg-Si alloys with a mole ratio of Mg to Si higher than 1.73, the Mg₂Si precipitates are distributed discontinuously, and there is no continuous corrosion channel, showing that the alloy is not sensitive to intergranular corrosion.

3) There exist Mg₂Si precipitates and coarse Si particles at the grain boundary of Al-Mg-Si alloys with a mole ratio of Mg to Si less than 1.73. Corrosion initiates on the Mg₂Si surface and at the PFZ at the adjacent periphery of Si particle. As corrosion time is extended, Si particle leads to severe anodic dissolution and corrosion of the PFZ at its adjacent periphery. Meanwhile, the Si particle also accelerates the preferential dissolution of Mg in Mg₂Si precipitate, expedites the polarity transformation between Mg₂Si and the PFZ, therefore the corrosion of the PFZ at the adjacent periphery of Mg₂Si precipitate is enhanced.

References

- GUILLAUMIN V, MANKOWSKI G. Localized corrosion of 6056
 T6 aluminium alloy in chloride media [J]. Corros Sci, 2000, 42:
 105-125
- [2] LARSEN M H, WALMSLEY J C. Intergranular corrosion of copper-containing AA6xxx AlMgSi aluminum alloys [J]. Journal of the Electrochemical Society, 2008, 155(11): C550–C556.
- [3] AMBAT R, DAVENPORT A J, SCAMANS G M, AFESETH A. Effect of iron-containing intermetallic particles on the corrosion behaviour of aluminium [J]. Corros Sci, 2006, 48: 3455–3471.
- [4] CUI Wen-fang, SUN Qiu-xia, CUI Jian-zhong. Study corrosion resistance of 01420 Al-Li alloy [J]. Rare Metal Materials and Engineering, 1995, 24(2): 40–44. (in Chinese)
- [5] ECKERMANN F, SUTER T, UGGOWITZER P J, AFESETH A. The influence of MgSi particle reactivity and dissolution processes on corrosion in Al-Mg-Si alloys [J]. Electrochimica Acta, 2008, 54: 844–855.
- [6] LI Jin-feng, ZHANG Zhao, CHENG Ying-liang, CAO Fa-he, ZHANG Jian-qing, CAO Chu-nan. Effect of aging state on localized corrosion of Al-4.0Cu-1.0Li-0.4Mg-0.4Ag-0.14Zr alloy in 3.0% NaCl solution [J]. The Chinese Journal of Nonferrous Metals, 2002, 12(5): 967–971. (in Chinese)
- [7] SVENNINGSEN G, LEIN J E, BJRGUM A, NOROLIEN J H, YU Y D, NISANCIOGLU K. Effect of low copper content and heat treatment on intergranular corrosion of model AlMgSi alloys [J]. Corrosion Science, 2006, 48: 226–242.
- [8] SVENNINGSEN G, LARSEN M H, NORDLIEN J H, NISANCI-OGLU K. Effect of high temperature heat treatment on intergranular corrosion of AlMgSi(Cu) model alloy [J]. Corros Sci, 2006, 48: 258–272.
- [9] AHLATCI H. Wear and corrosion behaviours of extruded Al-12Si-xMg alloys [J]. Materials Letters, 2008, 62: 3490–3492.
- [10] WANG Zhu-tang, TIAN Rong-zhang. Handbook of aluminum alloy and fabrication [M]. 2nd ed. Changsha: Central South University Press, 2000. (in Chinese)
- [11] BRIBILIS N, BUCHHEIT R G Electrochemical characteristics of intermetallic phases in aluminum alloys [J]. J Electrochem Soc, 2005, 152(4): B140–B151.
- [12] LI J F, ZHENG Z Q, LI S C, CHEN W J, REN W D, ZHAO X S. Simulation study on function mechanism of some precipitates in localized corrosion of Al alloys [J]. Corros Sci, 2007, 49: 2436–2449.
- [13] LI Jin-feng, PENG Zhuo-wei, LI Chao-xing, JIA Zhi-qiang, CHEN Wen-jing, ZHENG Zi-qiao. Mechanical properties, corrosion behaviors and microstructures of 7075 aluminium ally with various aging treatments [J]. Transactions of Nonferrous Metals Society of China, 2008, 18: 755–762.

- [14] LI Jin-feng, ZHENG Zi-qiao, REN Wen-da, CHEN Wen-jing, ZHAO Xu-shan, LI Shi-chen. Simulation on function mechanism of T₁(Al₂CuLi) precipitate in localized corrosion of Al-Cu-Li alloys [J]. Transactions of Nonferrous Metals Society of China, 2006, 16: 1268–1273
- [15] BUCHHEIT R G, GRANT R P, HLAVA P F, MCKENIIE B, IENDER G L. Local dissolution phenomena associated with S phase (Al₂CuMg) particles in aluminum alloy 2024-T3 [J]. J Electrochem
- Soc. 1997, 144(8): 2621-2628.
- [16] SHAO M H, FU Y, HU R G, et al. A study on pitting corrosion of aluminum alloy 2024-T3 by scanning microreference electrode technique [J]. Mater Sci Eng A, 2003, 344: 323–327.
- [17] LI Jin-feng, ZHENG Zi-qiao, JIANG Na, TAN Cheng-yu. Study on localized corrosion mechanism of 2××× series Al alloy containing S(Al₂CuMg) and θ'(Al₂Cu) precipitates in 4.0% NaCl solution at pH=6.1 [J]. Mater Chem Phys, 2005, 91(2–3): 325–329.

Al-Mg-Si 合金中 Mg₂Si 和 Si 粒子 在晶间腐蚀过程中的作用机理

曾锋利1,卫中领2,李劲风1,李朝兴1,谭星1,张昭3,郑子樵1

- 1. 中南大学 材料科学与工程学院,长沙 410083; 2. 嘉兴市轻合金技术重点实验室,嘉兴 314000; 3. 浙江大学 化学系,杭州 310027
- 摘 要:研究 Al-Mg-Si 合金晶界组成相($Al-Mg_2Si$ 及 $Al-Mg_2Si-Si$)间的电化学行为和动态电化学耦合行为,提出 Al-Mg-Si 合金的晶间腐蚀机理。研究表明,晶界 Si 的电位比其边缘 Al 基体的正,在整个腐蚀过程中作为阴极导致其边缘 Al 基体的阳极溶解;晶界 Mg_2Si 的电位比其边缘 Al 基体的负,在腐蚀初期作为阳极发生阳极溶解,然而由于 Mg_2Si 中活性较高的元素 Mg 的优先溶解,不活泼元素 Si 的富集,致使 Mg_2Si 电位正移,甚至与其边缘 Al 基体发生极性转换,导致其边缘 Al 基体的阳极溶解。当 n(Mg)/n(Si) < 1.73 时,随着腐蚀的进行,合金晶界同时会有 Mg_2Si 析出相和 Si 粒子,腐蚀首先萌生于 Mg_2Si 相和 Si 边缘的无沉淀带,而后,Si 粒子一方面导致其边缘无沉淀带严重的阳极溶解,另一方面加速 Mg_2Si 和晶界无沉淀带的极性转换,从而促使腐蚀沿晶界 Si 粒子及 Mg_2Si 粒子边缘向无沉淀带发展。

关键词: Al-Mg-Si 合金; 晶间腐蚀; 腐蚀机理; 电化学行为; Mg₂Si; Si

(Edited by YANG Hua)